Fujioka *et al.*
Progress in Earth and Planetary Science (2022) 9:31
https://doi.org/10.1186/s40645-022-00488-1

Progress in Earth and Planetary Science

RESEARCH ARTICLE Open Access

Depth profile of frictional properties in the inner Nankai accretionary prism using cuttings from IODP Site C0002

Riho Fujioka[1,6], Ikuo Katayama[1*], Manami Kitamura[2], Hanaya Okuda[3,4] and Takehiro Hirose[5]

Abstract

We conduct frictional experiments using cuttings collected at Nankai Trough IODP Site C0002 over 980.5–3262.5 mbsf (meters below seafloor) depth interval to better understand the frictional properties through the accretionary prism. The experiments are conducted at the in situ effective normal stresses (9–37 MPa) under brine-saturated conditions, and the slip velocity is abruptly changed in a stepwise manner to either of 0.3, 3, or 33 μm/s after the steady-state friction is reached. The friction coefficient (μ) of the cuttings samples ranges from 0.45 to 0.60, with a slight increase in μ with increasing depth, related to decreasing smectite content. The velocity dependence of friction ($a - b$) is positive at all depths and ranges from 0.001 to 0.006, which indicates a velocity-strengthening behavior; these values are consistent with relatively homogeneous deformation microstructures. The critical slip distance (D_c) ranges from 0.5 to 123 μm, with relatively large values obtained for the smectite-rich samples. The changes in both the friction coefficient and rate- and state-friction parameters are likely associated with mineralogical change and consolidation with increasing depth. Although all of the cuttings samples collected from Site C0002 exhibit a velocity-strengthening behavior, a slight decreasing trend in $a - b$ with increasing depth indicates either a nearly neutral velocity dependence or a possible transition to velocity-weakening behavior at greater depths, which may be attributed to the occurrence of slow earthquakes in the Nankai accretionary prism.

Keywords: Nankai Trough, Friction coefficient, Velocity dependence of friction, Clay minerals, Accretionary prism

1 Introduction

Nankai megathrust earthquakes have occurred repeatedly at approximately 100–150-year intervals and have historically been devastating events (Ando 1975; Hori et al. 2004). The 1944 Showa-Tonankai Earthquake and 1946 Showa-Nankai Earthquake were the most recent major earthquakes that occurred in the Nankai Trough. Slow earthquakes, including slow-slip events (SSEs) and very low-frequency earthquakes (VLFEs), have also been observed in shallow parts of the Nankai Trough accretionary prism (e.g., Ito and Obara 2006; Sugioka et al. 2012; Araki et al. 2017; Yokota and Ishikawa 2020; Shiraishi et al. 2020). Since slow earthquakes are sensitive to small changes in stress such as tidal stress, they can potentially serve as an indicator of the stress level and contribute to our understanding of megathrust earthquake processes (Obara and Kato 2020). The Nankai Trough Seismogenic Experiment (NanTroSEIZE) was conducted in 2007–2019 as part of the Integrated Ocean Drilling Program/International Ocean Discovery Program (IODP) to better understand the seismogenesis of Nankai Trough earthquakes. In this project, the D/V *Chikyu* drilled toward the plate boundary fault, where great earthquakes and tsunamis have been repeatedly generated, and collected sediment samples from the accretionary prism, measured various physical

*Correspondence: katayama@hiroshima-u.ac.jp
[1] Department of Earth and Planetary Systems Science, Hiroshima University, Hiroshima 739-8526, Japan
Full list of author information is available at the end of the article

properties, and installed sensors to monitor conditions at the drilled sites.

Core samples and cuttings were collected at various locations across the Nankai Trough during the NanTroSEIZE expeditions. Site C0002, the centerpiece of the broader NanTroSEIZE Kumano transect, reached the maximum depth of 3262.5 m below the seafloor (mbsf) in the Nankai accretionary prism (Tobin et al. 2020). A series of core samples were successfully recovered at Site C0002; however, coring was limited to the 475–1057, 2163–2218.5, and 2816.5–2848.5 mbsf intervals (Tobin et al. 2015, 2020). Takahashi et al. (2014) conducted triaxial deformation experiments using the core samples collected from the shallow interval at Site C0002 (< 1049 mbsf) and demonstrated that the friction coefficient was closely related to the clay mineral content. Okuda et al. (2021) found a velocity dependence on the frictional behavior of a deep core sample (2840.5 mbsf) from Site C0002, with velocity-strengthening behavior at slip velocities of > 10 μm/s, whereas velocity-weakening behavior is dominant at lower slip velocities. Although these experimental data are vital in advancing our understanding of the slip behavior in the Nankai accretionary prism, the limited coring intervals do not provide the depth variation of frictional properties through the accretionary prism. However, cuttings samples were continuously collected from the circulating drilling mud over the 875–3262.5 mbsf interval at Site C0002 during the riser operations for Expeditions 338, 348, and 358. In this study, we use cuttings samples from every 50 m depth interval over the 980.5–3262.5 mbsf range to establish a continuous depth profile of the frictional properties in the inner Nankai accretionary prism. We conducted laboratory experiments at in situ effective normal stresses under brine-saturated conditions, and we use the rate- and state-dependent constitutive friction law to analyze the frictional behavior. We then discuss the slip behavior in the accretionary prism and its spatial variations in the Nankai Trough.

2 Samples and methods

2.1 Geological setting

The Nankai Trough is a convergent plate margin where the Philippine Sea Plate subducts beneath the Eurasian Plate at a subducting rate of 4–6.5 cm/year (Heki and Miyazaki 2001; Loveless and Mead 2010). Site C0002 is located off the Kii Peninsula (Fig. 1), within the Kumano Basin and inner Nankai accretionary prism. The lithologies observed at this site are divided into five major units: Units I–III are in the Kumano forearc basin (above 975.5 mbsf), and Units IV and V are in the inner accretionary prism (e.g., Tobin et al. 2015). In this study, we used the cuttings samples collected from Units IV and V in the accretionary prism. Unit IV is dominated by silty claystone, with rare interbedded sandstone, and is interpreted as an older accretionary prism that consists of accreted Shikoku Basin hemipelagic and/or trench sediments. Unit V is dominated by silty claystone and is considered to be Shikoku Basin hemipelagic and/or trench sediments that were deposited during the Miocene (Tobin et al. 2015).

2.2 Sample descriptions

The cuttings samples used in this study were selected at every 50 m from the depth interval over the 980.5–3262.5 mbsf range at Holes C0002N, C0002P, and C0002Q (Fig. 2). The cuttings were washed with natural seawater at the drilling site to remove any residual drilling mud, and intact cuttings were then hand-picked to avoid any altered samples from their original state, following the approach outlined in Kitamura et al. (2021). The cuttings were dried in an oven at 40 °C for at least 24 h, then crushed, and sieved to produce gouge powder with a < 106 μm particle size. The total clay mineral, smectite, and illite contents of the cuttings samples from Holes C0002N and C0002P were taken from the X-ray diffraction data reported by Underwood (2017a, b), and the clay mineral content of the cuttings from Hole C0002Q was taken from Kitajima et al. (2020). The total clay mineral content is the sum of the smectite, illite, kaolinite, and chlorite contents. The smectite content decreased from Units IV to V and ranged of 6 to 35 wt% range. Conversely, the illite content exhibited relatively large variations and spanned the 13–36 wt% range, with an increase in illite content with increasing depth below 2500 mbsf (Fig. 2).

2.3 Experimental method

Frictional experiments were conducted using the biaxial frictional machine at Hiroshima University, Japan, under fluid-saturated conditions using an NaCl solution that simulated seawater (0.5 mol/L) at room temperature. The details of the experimental procedures can be found in Noda and Shimamoto (2009) and Katayama et al. (2015). The experiments were conducted at in situ effective normal stresses corresponding to the sample depths ($\sigma_{eff} = 9–37$ MPa), which were calculated from the difference between the lithostatic overburden pressure and hydrostatic pore pressure (Fig. 2). The overburden pressure and hydrostatic pressures were obtained by integrating the bulk densities of the collected sediments and seawater, respectively. The gouge sample was sandwiched between gabbro blocks in a double-direct shear configuration, in which the thickness of the simulated gouge layer was initially ~ 0.5 mm. The assembly was placed in the water

tank filled with brine and pre-compacted for 1 h at 2.5 MPa, and then normal stress was increased to the target value and kept for another 1 h before deformation (Fig. 3). The two-stage compaction was carried to prevent an excess pore pressure in the gauge layer. In this apparatus, pore fluid pressure cannot be controlled, such that we applied the in situ effective normal stresses as the normal stress under fluid-saturated conditions. The shear stress was applied downward from the upper piston to shear the simulated fault surfaces. After steady-state slip behavior was achieved at 8 mm displacement using a constant slip velocity of 3 μm/s, the slip velocity was changed abruptly in a stepwise manner among 0.3, 3, and 33 μm/s to analyze the rate- and state-dependent frictional behavior (velocity step test). The mechanical data were recorded using a KYOWA data recorder (EDX-100A) at 10 Hz sampling rate. The axial displacement was monitored by the electromagnetic transducer and corrected by the machine stiffness (4.4×10^8 N/m). The steady-state friction coefficient (μ) and the velocity-dependent parameters ($a - b$ and D_c), which are defined by the rate- and state-dependent friction law (e.g., Dieterich 1979; Ruina 1983), were examined during these experiments.

The friction coefficient μ can be calculated as the shear stress τ divided by the effective normal stress σ_{eff}:

$$\mu = \frac{\tau}{\sigma_{\mathrm{eff}}}. \tag{1}$$

The rate- and state-dependent friction law used in this study is expressed as:

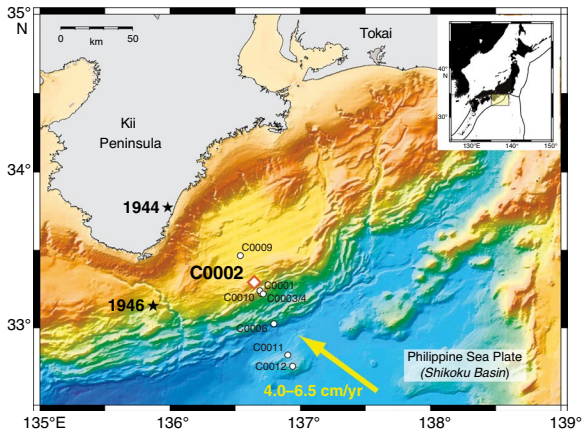

Fig. 1 Map of the NanTroSEIZE drilling sites. Site C0002 is indicated by the red square, and white circles mark the other NanTroSEIZE sites (after Tobin et al. 2015). Yellow arrows denote the estimated far-field vectors between the Philippine Sea Plate and Japan (Heki and Miyazaki 2001). Stars mark the hypocenters of the 1944 and 1946 great earthquakes

$$\mu(V,\theta) = \mu_0 + a\ln\left(\frac{V}{V_0}\right) + b\ln\left(\frac{V_0\theta}{D_c}\right), \tag{2}$$

where μ_0 is the initial friction coefficient before the velocity step; V_0 and V are the slip velocities before and after changes in slip velocity; a and b are nondimensional parameters that define the velocity dependence of the friction coefficient; D_c is the critical slip distance; and θ is a time-dependent state variable (e.g., Dieterich 1979; Ruina 1983). We used the one state variable version of the rate- and state-dependent friction law in this study. We used the aging law for the time evolution of θ, which is expressed as:

$$\frac{d\theta}{dt} = 1 - \frac{V\theta}{D_c}. \tag{3}$$

When the steady state is reached after the velocity step from V_0 to V (i.e., $d\theta/dt = 0$, such that $\theta = D_c/V$), the steady-state friction coefficient at slip velocity V is expressed as:

$$\mu_{ss} = \mu_0 + (a-b)\ln\left(\frac{V}{V_0}\right). \tag{4}$$

The velocity dependence of $a - b$ is then obtained as:

$$a - b = \frac{\Delta\mu_{ss}}{\Delta lnV}, \tag{5}$$

where $\Delta\mu_{ss} = \mu_{ss} - \mu_0$ and $\Delta\ln V = \ln(V/V_0)$. $a - b$ in an indicator of whether the frictional sliding is stable or unstable; $a - b < 0$ indicates velocity-weakening and potentially unstable slip that can evolve into an earthquake, whereas $a - b > 0$ indicates velocity-strengthening and stable slip. We obtained the velocity-dependent parameters by analyzing the data from the velocity upstep using the RSFit3000 software (Skarbek and Savage 2019). The analyzed frictional properties were compared with the clay contents reported by Underwood (2017a, b) and Kitajima et al. (2020). If mineral data were not available at the same depth, we used the closest data to our samples when the depth difference was < 5 m.

3 Results

3.1 Friction coefficient (μ)

We conducted 46 experiments using the cuttings obtained from Holes C0002N, C0002P, and C0002Q (Table 1). Most experiments exhibited slip-hardening, such that the friction coefficient increases slightly with displacement (Fig. 4). Friction coefficient for each sample was calculated at a displacement of 8 mm and was in the 0.45–0.60 range, with a slight increase in μ

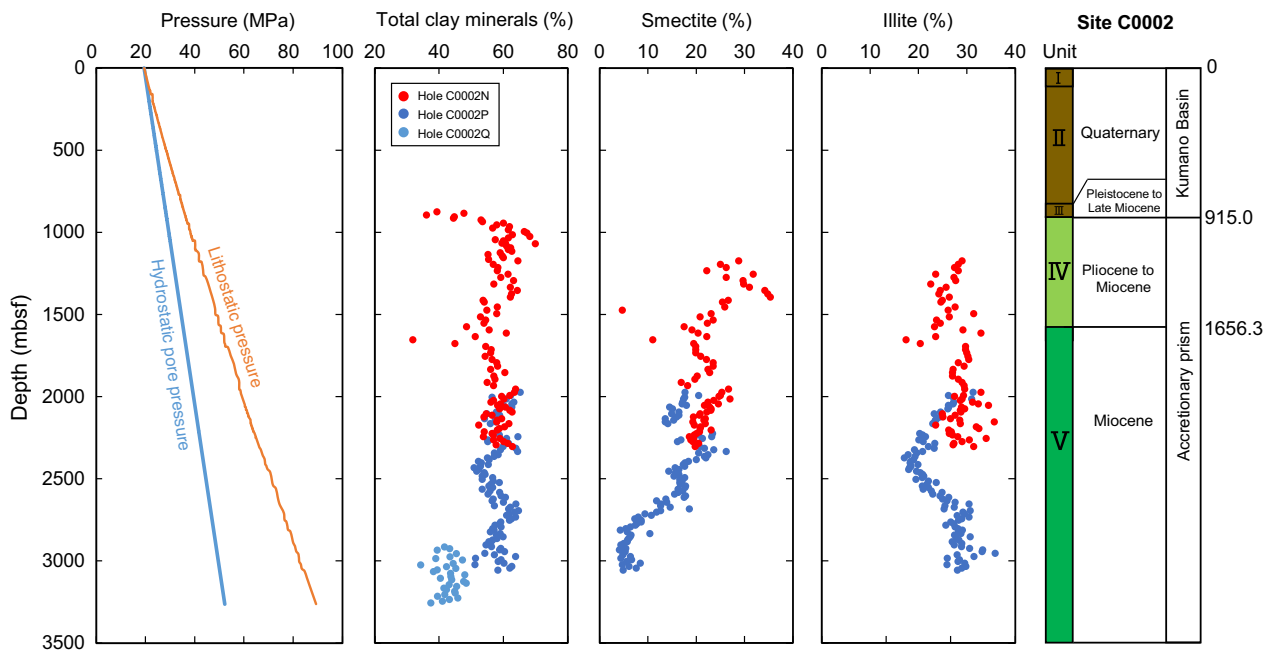

Fig. 2 Pressure, clay mineral content, and unit classification profiles for Site C0002 (after Tobin et al. 2015, 2020; Underwood 2017a, b; Kitajima et al. 2020). The lithospheric pressure is calculated from the overburden stress, which is derived from the rock density, and the hydrostatic pore pressure is calculated using a fluid density of 1.024 g/cm^3

with increasing depth (Fig. 5). We obtained μ values of 0.45–0.54, 0.46–0.60, and 0.48–0.54 for Holes C0002N, C0002P, and C0002Q, respectively. There were relatively small variations in μ throughout Holes C0002N and C0002Q, whereas the samples from Hole C0002P exhibited relatively large variations in μ, with a general increase in μ with increasing depth. Previous experiments that analyzed the Site C0002 core samples reported μ values of 0.53–0.55 in the shallow depth interval (Takahashi et al. 2014; Okuda et al. 2021), which is consistent with our data; however, the results at the deeper intervals yielded a lower value ($\mu = 0.41$) than those obtained in this study. Bedford et al. (2021) have recently reported μ values of 0.37–0.45 using the cutting samples collected from the 3212.5–3217.5 mbsf interval. The differences in friction coefficient among these different studies for the deeper intervals of Site C0002 are likely caused by slip-hardening behavior, because the samples exhibited a slight increase in μ as the displacement increased. We showed that the variation of friction coefficient calculated at different displacements (Fig. 5), indicating that those calculated at a similar small displacement are mostly consistent with previous experiments.

3.2 Velocity dependence parameters ($a - b$ and D_c)

The velocity steps yielded positive $a - b$ values for all of cuttings samples at Site C0002, with $a - b$ in the 0.001–0.006 range (Fig. 6A). There was no systematic difference in $a - b$ among the different hole, with $a - b$ values in the 0.002–0.006, 0.001–0.005, and 0.002–0.005 for Holes C0002N, C0002P, and C0002Q, respectively. The resultant $a - b$ for the upstep velocity to 33 μm/s was slightly larger than that for the upstep velocity to 3 μm/s. There was a slight decrease in $a - b$ with increasing depth toward a neutral value, especially in the case of the upstep velocity to 3 μm/s. These positive $a - b$ observations are consistent with previous studies at Site C0002 (Takahashi et al. 2014; Okuda et al. 2021; Bedford et al. 2021), although Okuda et al. (2021) reported that $a - b$ can be negative at relatively low slip velocities (≤ 1 μm/s). Our experiments were conducted under brine-saturated condition, with no control on the pore (atmospheric) pressure; however, Bedford et al. (2021) tested a range of pore pressures and found a slight increase in $a - b$ with increasing pore fluid pressure.

The critical slip distance (D_c) was between 0.5 and 123 μm and generally decreased with depth (Fig. 6B). D_c tended to be larger for higher slip velocity. These values largely agree with those obtained by previous studies at Site C0002 (Okuda et al. 2021; Bedford et al. 2021). Bedford et al. (2021) reported that D_c was relatively insensitive to the pore pressure but increased with increasing effective normal stress. However, our depth profile exhibited a nearly constant D_c below ~ 2000 mbsf, with

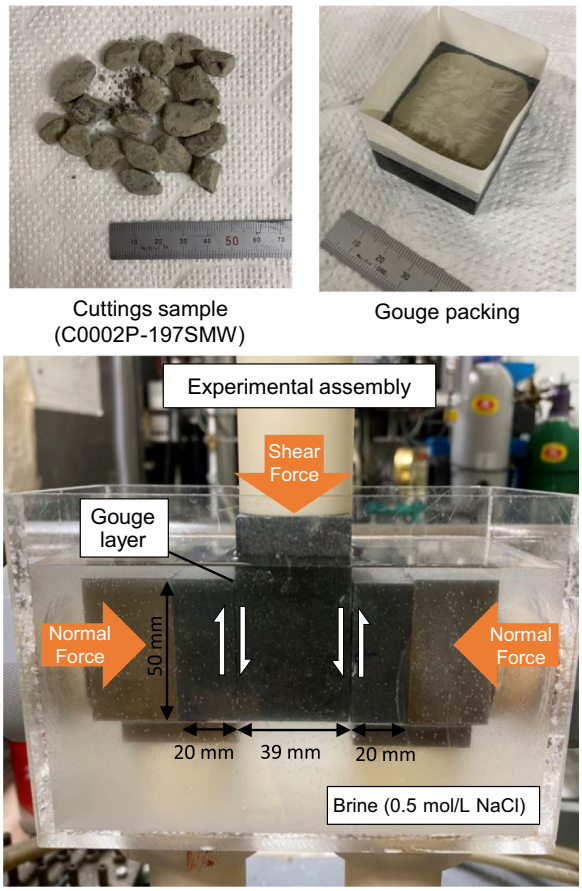

Fig. 3 Photographs of the cutting samples, preparation of the simulated gouges, and experimental apparatus. The experiments were conducted under fluid-saturated conditions using a 0.5 mol/L NaCl solution

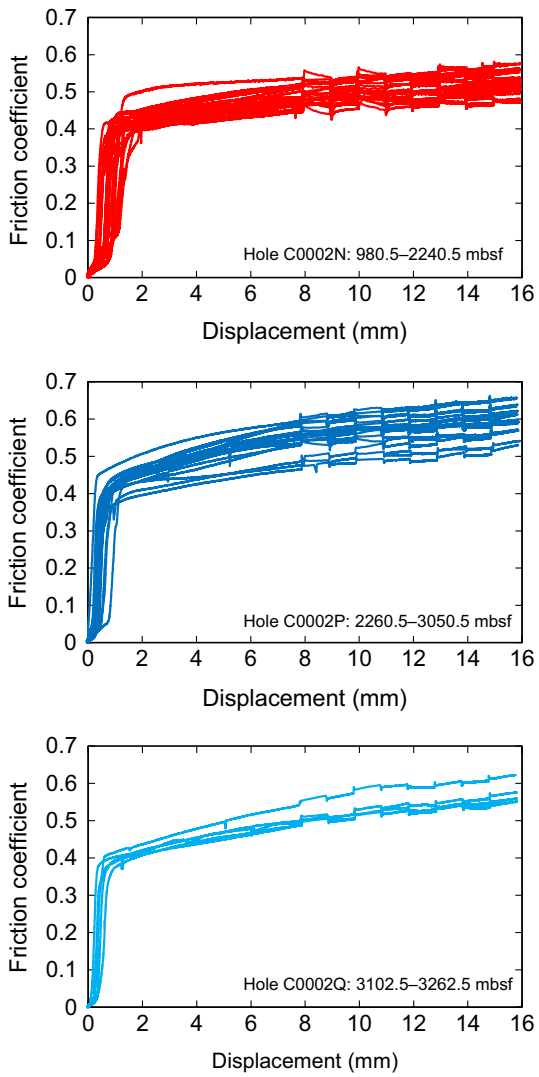

Fig. 4 Results of the frictional experiments of the cuttings samples collected from Holes C0002N (980.5–2240.5 mbsf), C0002P (2260.5–3050.5 mbsf), and C0002Q (3102.5–3262.5 mbsf). The experiments were run at a slip velocity of 3 μm/s for the first 8 mm of displacement, followed by stepwise changes of 0.3, 3, and 33 μm/s to test the velocity dependence of friction

effective normal stresses in the 20–37 MPa range, which may be influenced by clay mineral variations.

3.3 Microstructure observations

We observed the microstructures of the C0002N-141SW (1510.5 mbsf, Hole C0002N) and C0002P-266SW (2560.5 mbsf, Hole C0002P) samples after the experiments (Fig. 7). The entire gouge layer of each sample was deformed and possessed abundant Riedel shear bands. Both samples exhibited a positive velocity dependence, and there was no systematic difference in the frictional behaviors of these two samples, even though they are from different depths. Homogeneous deformation microstructures, like those observed in Fig. 7, are typical for velocity-strengthening materials, whereas highly localized deformation is more common in velocity-weakening materials (e.g., Beeler et al. 1996).

4 Discussion

4.1 Relationship between the frictional properties and clay mineral content

The frictional properties that were determined using our experimental data were compared with the clay mineral contents of the cuttings samples reported by Underwood et al. (2017a; b) and Kitajima et al. (2020). Figure 8 shows the relationship between the friction coefficients and the total clay mineral and smectite contents, including previous experimental data from samples collected along the Kumano transect in the Nankai Trough. Our

Table 1 Summary of the experimental results

Exp. run number	Sample source	Bottom depth (mbsf)	Effective pressure (MPa)	Slip rate (μm/s)	Friction coefficient	$a-b$ (3 to 33 μm/s)	$a-b$ (0.3 to 3 μm/s)	D_c (μm) (3 to 33 μm/s)	D_c (μm) (0.3 to 3 μm/s)
HTB742	C0002N-25SMW	980.5	8.6	0.3, 3, 33	0.48	0.0027	0.0053	75.0	9.2
HTB733	C0002N-35SMW	1030.5	9	0.3, 3, 33	0.52	0.0049 ± 0.0003	0.0043	53.9 ± 23.9	15.1
HTB730	C0002N-56SMW	1130.5	10.9	0.3, 3, 33	0.54	0.0056 ± 0.0009	0.0063 ± 0.0003	112.4 ± 55.8	17.6 ± 12.4
HTB726	C0002N-66SMW	1180.5	11.5	0.3, 3, 33	0.47	0.0038 ± 0.0001	0.0034 ± 0.0008	123.3 ± 5.7	43.5 ± 13.5
HTB724	C0002N-82SMW	1230.5	11.6	0.3, 3, 33	0.52	0.0038	0.0031 ± 0.0001	29.8	3.3 ± 3.2
HTB723	C0002N-98SMW	1310.5	12.8	0.3, 3, 33	0.46	0.0037 ± 0.0001	0.0037 ± 0.0007	115.6 ± 4.4	43.4 ± 21.0
HTB720	C0002N-110SMW	1360.5	13.3	0.3, 3, 33	0.48	0.0048 ± 0.0001	0.0042	41.2 ± 11.2	9.4
HTB719	C0002N-120SMW	1410.5	13.8	0.3, 3, 33	0.46	0.0031 ± 0.0016	0.0035 ± 0.0005	111.8 ± 12.2	48.5 ± 23.9
HTB713	C0002N-141SMW	1510.5	14.9	0.3, 3, 33	0.50	0.0041 ± 0.0002	0.0031	70.1 ± 6.7	26.7
HTB712	C0002N-153SMW	1560.5	14.6	0.3, 3, 33	0.52	0.0033 ± 0.0005	0.0039 ± 0.0001	79.2 ± 2.6	17.9 ± 3.2
HTB711	C0002N-163SMW	1610.5	15.2	0.3, 3, 33	0.45	0.0041 ± 0.0018	0.0041 ± 0.0009	91.5 ± 41.1	35.9 ± 34.5
HTB710	C0002N-185SMW	1700.5	17.0	0.3, 3, 33	0.49	–	–	–	–
HTB709	C0002N-196SMW	1750.5	17.6	0.3, 3, 33	0.48	0.0035 ± 0.0006	0.0036	76.0 ± 15.2	19.8
HTB702	C0002N-206SMW	1800.5	18.4	0.3, 3, 33	0.50	0.0047 ± 0.0001	0.0044	57.1 ± 24.9	10.4
HTB701	C0002N-227SMW	1900.5	19.5	0.3, 3, 33	0.52	0.0052 ± 0.0019	0.0026	26.3 ± 6.3	14.3
HTB700	C0002N-240SMW	1960.5	19.4	0.3, 3, 33	0.45	0.0058 ± 0.0002	0.0033	50.0 ± 20.0	15.0
HTB699	C0002N-251SMW	2000.5	20.3	0.3, 3, 33	0.47	0.0045 ± 0.0001	0.0039 ± 0.0002	64.9 ± 3.5	9.8 ± 2.9
HTB698	C0002N-263SMW	2030.5	20.1	0.3, 3, 33	0.49	0.0040 ± 0.0000	0.0027 ± 0.00002	25.0 ± 5.0	10.5 ± 2.3
HTB697	C0002N-267SMW	2050.5	20.4	0.3, 3, 33	0.51	0.0037 ± 0.0003	0.0023 ± 0.0003	40.0 ± 5.0	20.2 ± 4.8
HTB696	C0002N-275SMW	2090.5	20.9	0.3, 3, 33	0.49	0.0060	0.0030 ± 0.0002	0.7 ± 0.7	4.6 ± 1.6
HTB695	C0002N-280SMW	2110.5	21.1	0.3, 3, 33	0.45	0.0053 ± 0.0002	0.0046 ± 0.0002	12.0 ± 2.0	6.5 ± 3.3
HTB694	C0002N-290SMW	2160.5	21.6	0.3, 3, 33	0.48	0.0051 ± 0.0000	0.0046 ± 0.0002	5.9 ± 0.2	4.4 ± 3.1
HTB693	C0002N-299SMW	2190.5	22.1	0.3, 3, 33	0.47	0.0041	–	7.3	–
HTB691	C0002N-309SMW	2240.5	22.8	0.3, 3, 33	0.45	0.0044 ± 0.0001	0.0037 ± 0.0003	20.8 ± 4.8	9.3 ± 1.1
HTB746	C0002P-114SMW	2260.5	22.9	0.3, 3, 33	0.53	0.0020	0.0019 ± 0.0002	36.6	15.6 ± 0.0
HTB749	C0002P-126SMW	2310.5	23.7	0.3, 3, 33	0.48	0.0039 ± 0.0002	0.0031 ± 0.0003	45.1 ± 36	13.6 ± 8.6
HTB750	C0002P-137SMW	2360.5	24.5	0.3, 3, 33	0.54	0.0041 ± 0.0004	0.0013	16.7 ± 3.3	21.4

Table 1 (continued)

Exp. run number	Sample source	Bottom depth (mbsf)	Effective pressure (MPa)	Slip rate (μm/s)	Friction coefficient	$a-b$ (3 to 33 μm/s)	$a-b$ (0.3 to 3 μm/s)	D_c (μm) (3 to 33 μm/s)	D_c (μm) (0.3 to 3 μm/s)
HTB752	C0002P-150SMW	2410.5	25.0	0.3, 3, 33	0.56	0.0023 ± 0.0000	0.0024 ± 0.0003	28.8 ± 0.6	5.5 ± 0.7
HTB753	C0002P-162SMW	2460.5	26.6	0.3, 3, 33	0.57	0.0037 ± 0.0004	0.0020	39.9 ± 9.9	0.9
HTB754	C0002P-173SMW	2510.5	26.8	0.3, 3, 33	0.56	–	0.0020 ± 0.0001	–	5.5 ± 0.9
HTB756	C0002P-184SMW	2560.5	27.9	0.3, 3, 33	0.59	0.0029 ± 0.0005	0.0017 ± 0.0001	27.5 ± 7.5	10.8 ± 2.0
HTB757	C0002P-197SMW	2610.5	28.1	0.3, 3, 33	0.46	0.0036	0.0038	6.5	5.8
HTB758	C0002P-209SMW	2660.5	28.5	0.3, 3, 33	0.49	0.0047 ± 0.0001	0.0040	20.0	1.1
HTB759	C0002P-220SMW	2710.5	29.6	0.3, 3, 33	0.55	0.0037	0.0016	7.5	16.8
HTB760	C0002P-232SMW	2760.5	30.1	0.3, 3, 33	0.60	0.0030 ± 0.0003	0.0006 ± 0.0003	3.3 ± 0.14	8.4 ± 1.6
HTB761	C0002P-243SMW	2810.5	30.2	0.3, 3, 33	0.53	0.0031 ± 0.0001	0.0024 ± 0.0002	20.5 ± 2.89	8.8 ± 0.8
HTB763	C0002P-255SMW	2860.5	31.3	0.3, 3, 33	0.53	0.0042 ± 0.0000	0.0035 ± 0.0005	5.0 ± 0.01	5.0
HTB764	C0002P-266SMW	2910.5	32.0	0.3, 3, 33	0.55	0.0030	0.0027 ± 0.0000	28.9	7.2 ± 1.4
HTB766	C0002P-278SMW	2960.5	32.9	0.3, 3, 33	0.59	0.0023 ± 0.0003	0.0007 ± 0.0001	10.7 ± 2.04	7.2 ± 0.3
HTB767	C0002P-290SMW	3010.5	33.0	0.3, 3, 33	0.58	0.0032 ± 0.0002	0.0018 ± 0.0001	2.0 ± 0.17	17.5 ± 2.5
HTB768	C0002P-299SMW	3050.5	33.7	0.3, 3, 33	0.54	0.0043	0.0020 ± 0.0004	2.1	13.8 ± 6.2
HTB769	C0002Q-450SMW	3102.5	35.0	0.3, 3, 33	0.49	0.0047	0.0032 ± 0.0002	0.5	6.1 ± 1.3
HTB770	C0002Q-500SMW	3142.5	35.5	0.3, 3, 33	0.51	0.0044 ± 0.0003	0.0032 ± 0.0002	13.1 ± 10.68	11.2 ± 3.8
HTB773	C0002Q-540SMW	3182.5	36.1	0.3, 3, 33	0.49	0.0039 ± 0.0003	0.0020 ± 0.0006	33.5 ± 6.48	23.5 ± 8.4
HTB774	C0002Q-578SMW	3222.5	36.6	0.3, 3, 33	0.48	0.0041	0.0024 ± 0.0001	25.0	21.1 ± 8.9
HTB775	C0002Q-634SMW	3262.5	37.2	0.3, 3, 33	0.54	0.0038	0.0019 ± 0.0000	5.4	5.8 ± 1.2

results indicate no systematic correlation between μ and the total clay mineral content; however, there was a weak negative correlation between μ and smectite content (Fig. 8). This decrease in μ with increasing smectite content has also been reported in previous studies (e.g., Takahashi et al. 2014; Ikari et al. 2013a, 2018; Okuda et al. 2021; Oohashi et al. 2015). It is widely accepted that smectite is characterized by a significantly lower μ value than those for other clay minerals under fluid-saturated conditions (e.g., Moore and Lockner 2007; Ikari et al. 2007; Behnsen and Faulkner 2012; Tetsuka et al. 2018; Morrow et al. 2017). Tembe et al. (2010) reported a nearly linear decreasing trend of the frictional strength with increasing smectite content in the quartz-mixed gouge materials. Our samples possessed small μ variation for smectite contents up to 34%; however, studies that have analyzed Nankai samples with higher smectite contents (Takahashi et al. 2014; Ikari et al. 2018) have revealed that μ decreases to as low as ~ 0.1 when the samples contain ~ 50% smectite, which is close to the end-member μ value of fluid-saturated smectite. The overall frictional strength is therefore controlled by the presence of weak materials, such as smectite, in the matrix of sample. Such a lithological dependency of the friction coefficient has previously been reported in various clay-bearing materials that have been collected from the IODP projects (e.g.,

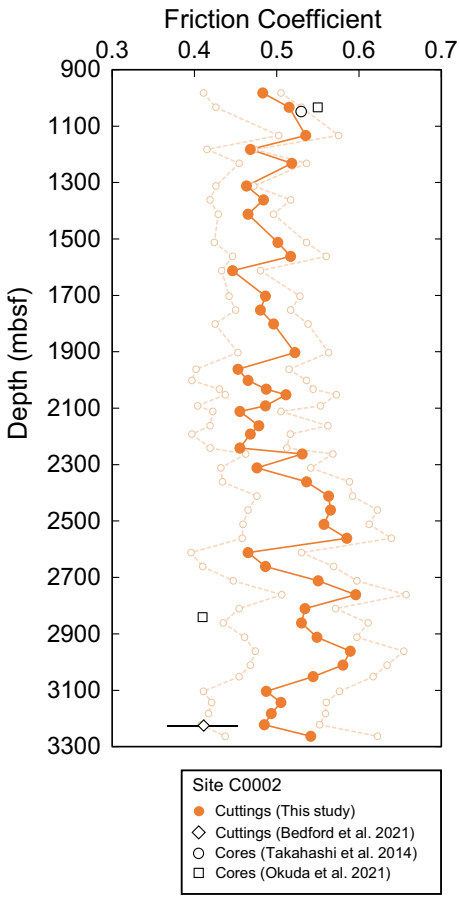

Fig. 5 Depth profile of the friction coefficient obtained via analysis of the cuttings at Site C0002. Friction coefficient obtained at a displacement of 8 mm is shown by orange filled circles, and the lower and upper data (orange open circle) are obtained at displacements of 2 mm and 16 mm, respectively. The black open circles, squares, and diamond indicate data from previous studies at Site C0002 (Takahashi et al. 2014; Okuda et al. 2021; Bedford et al. 2021)

Deng and Underwood 2001; Brown et al. 2003; Kopf and Brown 2003; Ikari et al. 2013b, 2018; Boulton et al. 2019). The Japan Trench Fast Drilling Project (JFAST) samples that were collected near the fault zone possessed μ values as low as ~0.2, which was significantly lower than those of the wall rocks ($\mu > 0.5$), with these variations attributed to different smectite contents (Ikari et al. 2015). The presence of such weak materials is thought to be crucial for the shallow trenchward slip of the 2011 Tohoku Earthquake (e.g., Remitti et al. 2015). Sedimentary samples that were collected from the Cocos Plate, Costa Rica, possessed large variation of friction coefficient, ranging from 0.2 to 0.8 (e.g., Kopf 2013; Namiki et al. 2014; Kurzawski et al. 2016). These variations have also been attributed to the different clay mineral contents and lithologies, which likely influenced the spatial variations in slip behavior in the Costa Rica subduction system.

Figure 9 shows the relationship between the velocity dependence of friction ($a - b$) and the total clay mineral and smectite contents. All of the samples exhibited a velocity-strengthening behavior ($a - b > 0$) and no systematic correlation with the total clay mineral content, but $a - b$ increased slightly with increasing smectite content. Clay-rich gouges commonly exhibit a positive velocity dependence (e.g., Morrow et al. 1992; Ikari et al. 2007; Tembe et al. 2010), which is in agreement with our results. This is likely due to the low or negative values of the rate parameter b in the case of clay-rich materials (Saffer and Marone. 2003). However, a negative velocity dependence of friction was reported for several Nankai sediment samples under low effective stresses (Tsutsumi et al. 2011) and at ultralow slip velocities (Ikari and Kopf 2017). Okuda et al. (2021) reported a velocity-weakening behavior for the samples collected from the Nankai Trough at slip velocities similar to our experiments, but their samples consisted of intact samples with slightly lower smectite contents.

Figure 10 shows the relationship between the critical slip distance (D_c) and clay mineral content. Although there were only limited total clay and smectite content variation in our samples, D_c tended to be larger for the sample with higher smectite contents. D_c is considered to be controlled primarily by the real contact area of the material surface (e.g., Dieterich and Kilgore 1994). D_c could be related to the rate parameter b, whereby both represent a change in the real contact area after the velocity step. The nearly maximized real contacts for weak and platy materials, such as clay minerals, may explain the relatively large D_c and the positive $a - b$ in the smectite-rich samples. Frictional healing experiments have shown a slower recovery rate and larger transient slip distance for smectite compared to the other minerals (Katayama et al. 2015). This is possibly due the weak creep strength of smectite, indicating a rapid growth of creeping and hence a nearly saturation in contact area after a short period. In contrast, the contact area for illite may be far from being saturated as suggested by the higher recovery rate of illite. Consequently, the slight decrease in D_c with increasing depth is likely attributed to the change in mineralogy from smectite-rich sediment to illite-rich sediment.

4.2 Implications for fault slip behavior in the Nankai Trough

A comparison of our results with those obtained at various locations along at the Kumano transect in the Nankai accretionary prism (e.g., Ikari and Saffer 2011; Takahashi et al. 2014; Ikari et al. 2013a; Okuda et al. 2021) is shown in Fig. 11. There are large variations in μ values of the Nankai samples, even at the same drilling sites. We show

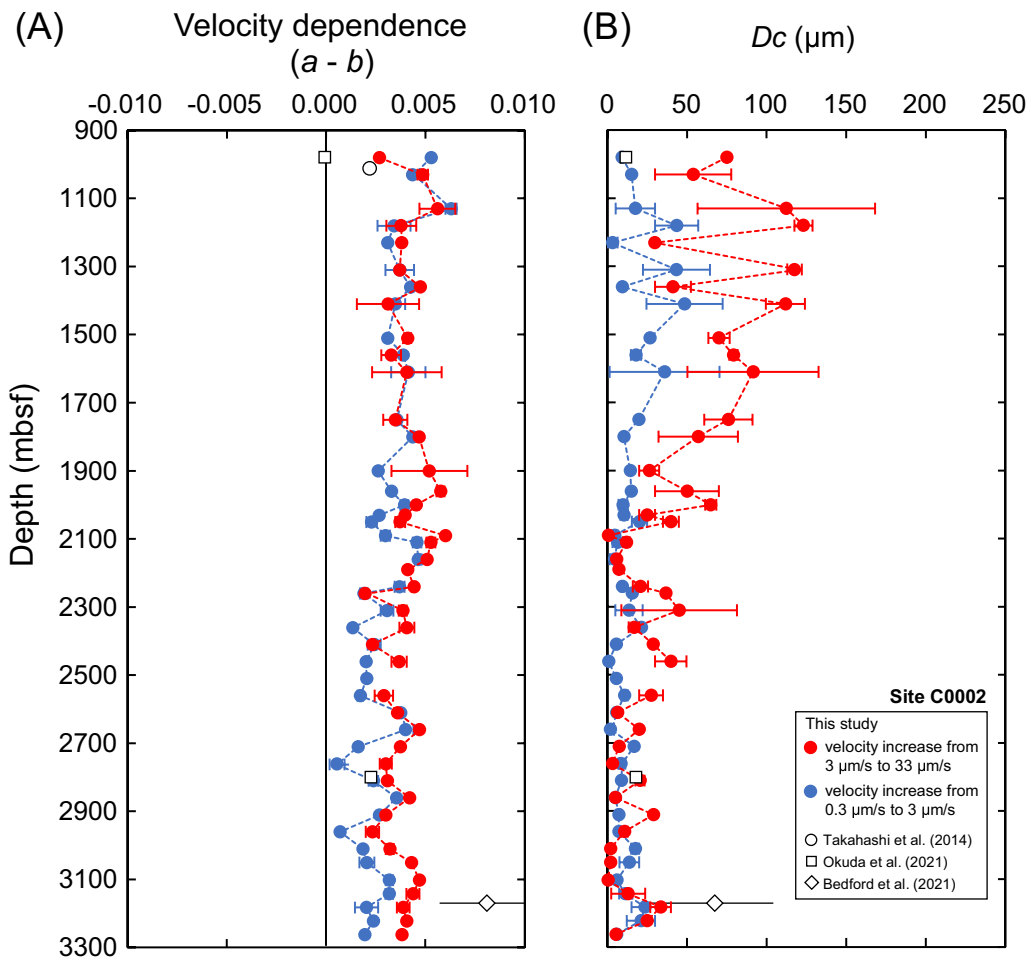

Fig. 6 Depth profiles of **A** the velocity dependence of friction $a - b$ and **B** critical slip distance D_c at Site C0002. Red and blue circles indicate the results for velocity change from 3 to 33 μm/s and from 0.3 to 3 μm/s, respectively. The error bars are estimated from the variations in the repeated tests. Open circles, squares, and diamond indicate data from previous studies at Site C0002 (Takahashi et al. 2014; Okuda et al. 2021; Bedford et al. 2021)

that our depth profile of the friction coefficient at Site C0002, where μ ranges from 0.45 at shallow depths to 0.6 at greater depths, possesses values that are slightly lower than those at Site C0009, which is located a few tens of kilometers landward in the accretionary prism (Takahashi et al. 2014). This difference could be attributed to the consolidation and lower abundance of smectite at C0009 due to diagenesis, as the mechanical strength of the sedimentary samples is highly sensitive to the degree of cementation (e.g., Schnaid et al. 2001; Ikari and Hüpers 2021). Samples from Site C0004/10, which is located in the outer prism where abundant splay faults are developed, possess lower μ values (0.22–0.48), with the intact samples possessing slightly higher μ values compared to the powder samples (Roesner et al. 2020). In these sites, the samples recovered from the fracture zones yielded markedly lower friction coefficient than those from the wall rocks (Ikari and Saffer 2011). Tsutsumi et al. (2011) reported relatively low μ values (0.28–0.49) at low slip velocities < 26 mm/s at Sites C0001 and C0004, although there was an abrupt drop in μ at slip velocities ≥ 26 mm/s. Conversely, the samples from the prism toe at Site C0006, and the incoming Philippine Sea Plate at Sites C0011 and C0012 possessed highly variable μ values, with 0.32–0.83 for the prism toe and 0.15–0.72 for the incoming sediments, which are likely due to the large lithological variations around these sites (Stipp et al. 2013; Ikari et al. 2013a, 2018; Okuda et al. 2021).

The velocity dependence of friction is also spatially variable in the Nankai accretionary prism. We show that all of the samples (down to 3262.5 mbsf) exhibit a velocity-strengthening behavior at relatively low slip

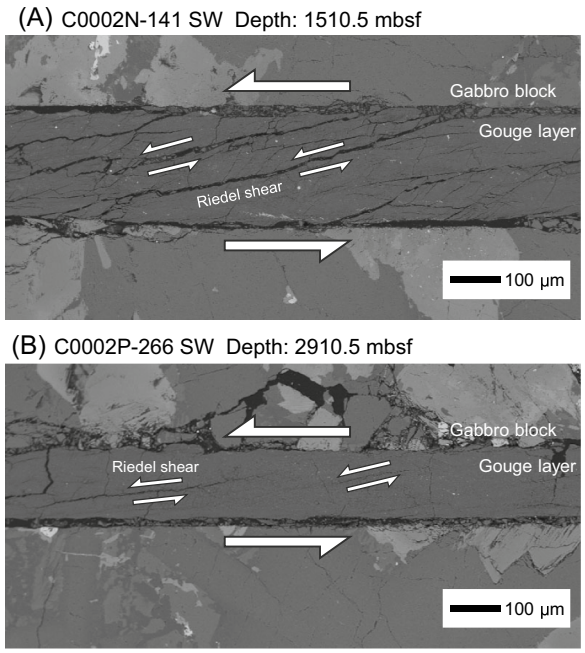

Fig. 7 Back-scattered electron images of the recovered samples **A** C0002N-141SW and **B** C0002P-266SW. The gouge layer is sandwiched between the gabbro forcing blocks, and the arrows in the blocks indicate slip directions. Riedel shears are widely developed in these samples. These images were taken using an electron-probe microanalyzer with a 15-kV accelerating voltage and 2.5 nA probe current

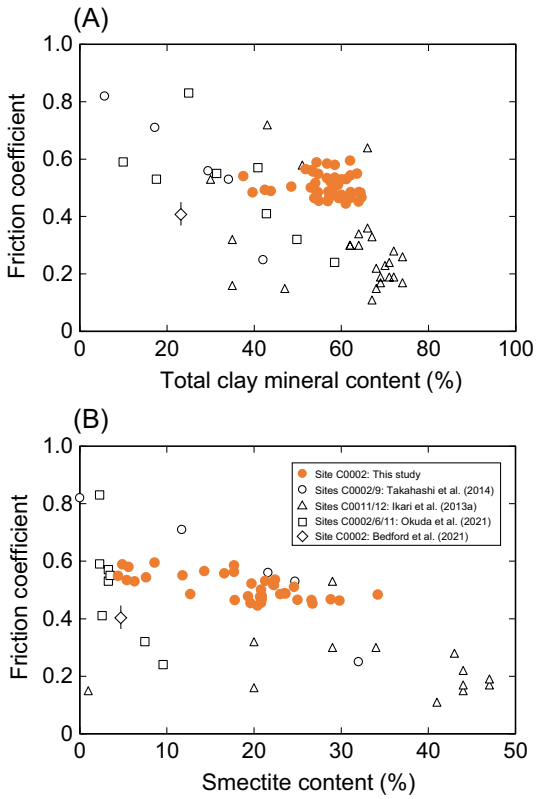

Fig. 8 Relationship between the friction coefficient and **A** total clay mineral content and **B** smectite content. Data obtained in this study are shown by orange circles, and open circles, triangles, squares, and diamond indicate data from previous studies of the Nankai samples collected along the Kumano transect (Takahashi et al. 2014; Ikari et al. 2013a; Okuda et al. 2021; Bedford et al. 2021)

velocities (up to 33 μm/s). This is in agreement with previous Site C0002 experimental results and with those from Site C0009, which is more landward in the inner accretionary prism (Takahashi et al. 2014). Therefore, the inner accretionary prism seems to be a region of stable slip, whereas the outer prism and further seaward regions exhibit a highly variable velocity dependence (Fig. 11). The fault zone materials collected at Site C0004 and C0010 possessed $a - b$ values in the -0.008 to 0.006 range, with the intact samples possessing a negative velocity dependence (Roesner et al. 2020). A velocity-weakening behavior is more common in the regions close to the trench at Site C0006 and further seaward at Site C0011 (Okuda et al. 2021). There are several factors that control the velocity dependence of friction, including lithification and consolidation (Moore and Saffer 2001; Ikari and Hüpers 2021), the effective normal stress (Moore and Saffer 2001; Bedford et al. 2021), shear localization (Saffer and Marone 2003; Ikari et al. 2011), and small-scale material heterogeneities (Bedford et al. 2022). We showed that $a - b$ decreased slightly with depth at Site C0002, which is in agreement with the lithification and consolidation model, although such a trend may also be attributed to a decrease in the smectite content and increase in the effective pressure with increasing depth. The velocity-weakening behavior is more widespread at shallow depths at Sites C0004, C0006, and C0011, such that various factors are needed to account for the complexity of these velocity dependences. Note that velocity dependence of friction can also be influenced by the sample preparation. The intact samples collected from the Nankai Trough exhibited velocity-weakening behavior in contrast to the powdered samples that favor velocity-neutral to velocity-strengthening behavior (Roesner et al. 2020). Although the intact materials are relevant for an incipient fault zone, the powered samples as those used in our experiments represent slip behavior of the mature fault zones where fault movements have created natural gouge.

Slow slip events (SSEs) and very low-frequency earthquakes (VLFEs) have been observed in the accretionary prism and décollement zone in the Nankai Trough (e.g., Ito and Obara 2006; Sugioka et al. 2012; Araki et al. 2017; Shiraishi et al. 2020). The slip rates of these slow earthquakes

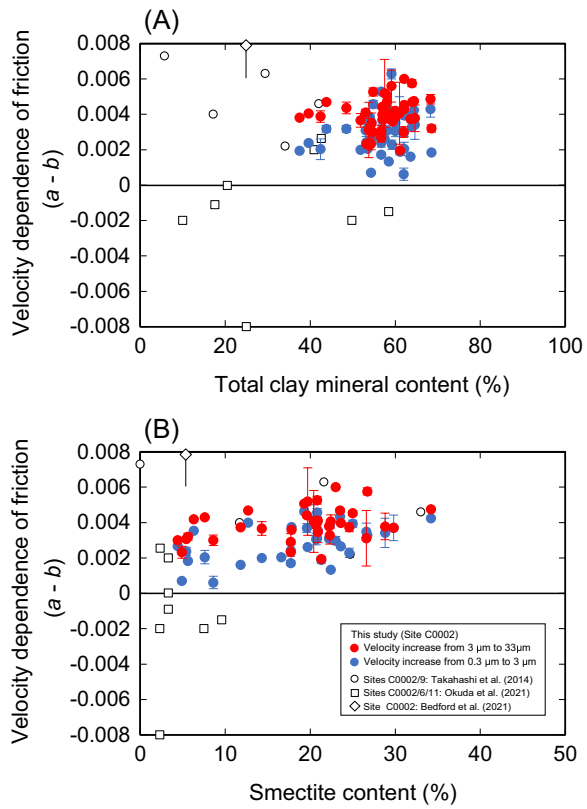

Fig. 9 Relationship between $a - b$ and **A** total clay mineral content and **B** smectite content. Red and blue circles indicate the results for velocity change from 3 to 33 μm/s and from 0.3 to 3 μm/s, respectively. Open circles, squares, and diamond indicate data from previous studies of the Nankai samples along the Kumano transect (Takahashi et al. 2014; Okuda et al. 2021; Bedford et al. 2021)

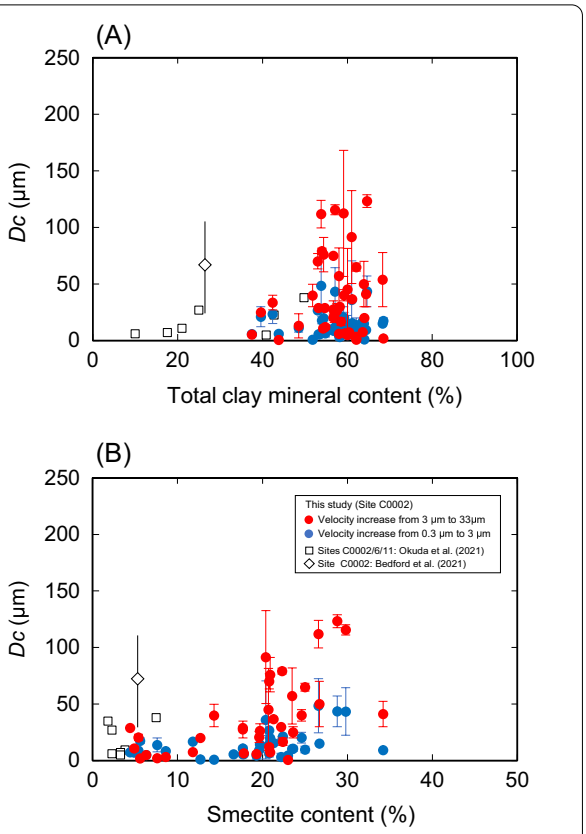

Fig. 10 Relationship between D_c and **A** total clay mineral content and **B** smectite content. Red and blue circles indicate the results for velocity change from 3 to 33 μm/s and from 0.3 to 3 μm/s, respectively. Open squares and diamond indicate data from previous studies of the Nankai samples along the Kumano transect (Okuda et al. 2021; Bedford et al. 2021)

(~1 m/day) are similar to those imposed in laboratory experiments, but the hypocentral depths are much deeper than the samples collected by the IODP projects. We show that $a - b$ tends to decrease with increasing depth (Fig. 6), with consolidation and mineralogical changes likely contributing to this decrease. Although our samples are limited to depths ≤ 3262.5 mbsf, a slight decrease in $a - b$ with depth may result in a neutral or negative value at greater depths. However, $a - b$ is dependent on various physicochemical properties including slip velocity, pore fluid pressure, temperature, structural developments, mineral assemblages, and their abundances (e.g., Marone 1998). In particular, temperature likely plays a key role in controlling the aseismic to seismic transition as temperature increases with depth in the accretionary prism. den Hartog and Spiers (2013) have shown that the transition from velocity strengthening to velocity weakening occurred at temperature of ~ 250 °C for illite-rich gouges under hydrothermal conditions. The transitional temperature is higher than that expected for the updip limit of seismogenic zone; however, relatively low nucleation velocities in nature compared to laboratory velocities may attribute to velocity weakening behavior at lower temperatures (den Hartog and Spiers 2013). In addition to velocity dependence of friction, fault stability is also influenced by critical slip distance, being more stable with a larger D_c (e.g., Scholz 2002). We show that D_c decreases slightly with depth, indicating that the shallow accretionary prism is relevant for stable region, whereas faults could become unstable at deeper portions due to the possible transition to negative velocity dependence with a small critical slip distance. Numerical modeling studies have favored such transitional slip behavior for the occurrence of slow earthquakes (e.g., Shibazaki and Shimamoto 2007; Rubin 2008). However, slow earthquakes may not be solely related to the rate-dependent friction, as the pore fluid pressure and associated effective normal stress on the fault zones are considered to be additional key factors for the slip instability in the Nankai accretionary prism (e.g., Kodaira et al. 2004; Hirose et al. 2021).

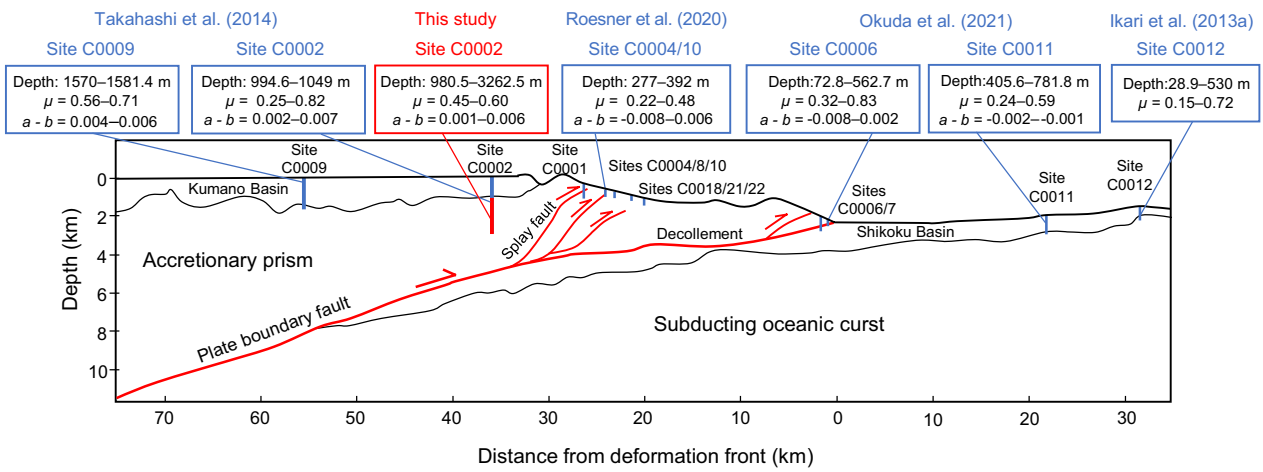

Fig. 11 Cross section of the Kumano transect across the Nankai accretionary prism (modified after Tobin et al. 2020), constructed using data from various drilling sites during the NanTroSEIZE expeditions, with the frictional properties at Sites C0002 (this study, Takahashi et al. 2014), C0009 (Takahashi et al. 2014), C0004/10 (Roesner et al. 2020), C0006 and C0011 (Okuda et al. 2021), and C0012 (Ikari et al. 2013a)

5 Conclusions

We conducted frictional experiments using cuttings samples that were obtained from 980.5 to 3262.5 mbsf at Nankai Trough Site C0002. The measured friction coefficients tended to increase slightly with increasing depth, which is likely controlled by the clay mineralogy, especially smectite content. The obtained velocity dependence of friction ($a - b$) indicated a velocity-strengthening behavior at all depths, which suggests that Site C0002 is a stable slip region, at least for the laboratory range of slip velocities tested here (0.3 to 33 μm/s). $a - b$ decreased slightly with increasing depth owing to consolidation and mineralogical changes, and the transition to velocity weakening may occur at greater depths. The occurrence of slow earthquakes in the Nankai accretionary prism may be associated with such transitional slip behavior.

Acknowledgements
We thank the crew, technicians, and science party on the D/V *Chikyu* for their work during the NanTroSEIZE expeditions. We also thank John Bedford and an anonymous reviewer for various comments, which greatly improved this manuscript. The samples that were analyzed in this study were provided by IODP. This work was partly supported by the IODP Expedition 348 After Cruise Research Program, Japan Agency for Marine-Earth Science and Technology (JAMSTEC) to MK.

Author contributions
RF and IK planned the project. MK and TH collected the samples. RF conducted the experiments, and RF, IK, and HO analyzed the data. All of the authors discussed the results and implications and approved the final version of the manuscript.

Funding
This research was supported by JSPS KAKENHI Grant Number JP16H06476 in Scientific Research on Innovative Areas "Science of Slow Earthquakes," JP20H00200, and JP20K04115.

Availability of data and material
Data sharing is not applicable to this article as no datasets were generated. Please contact the author for data requests.

Declarations

Competing interests
The authors declare that they have no competing interests.

Author details
[1]Department of Earth and Planetary Systems Science, Hiroshima University, Hiroshima 739-8526, Japan. [2]Geological Survey of Japan, National Institute of Advanced Industrial Science and Technology (AIST), Tsukuba, Ibaraki 305-8567, Japan. [3]Department of Ocean Floor Geoscience, Atmosphere and Ocean Research Institute, University of Tokyo, Kashiwa, Chiba 277-8564, Japan. [4]Department of Earth and Planetary Science, University of Tokyo, Bunkyo, Tokyo 113-0033, Japan. [5]Kochi Institute for Core Sample Research (X-Star), Japan Agency for Marine Earth Science and Technology (JAMSTEC), Nankoku, Kochi 783-8502, Japan. [6]Present Address: Marine Works Japan, Yokosuka, Kanagawa 237-0063, Japan.

Received: 18 February 2022 Accepted: 15 May 2022
Published online: 03 June 2022

References

Ando M (1975) Source mechanisms and tectonic significance of historical earthquakes along the Nankai Trough, Japan. Tectonophysics 27:119–140. https://doi.org/10.1016/0040-1951(75)90102-X
Araki E, Saffer DM, Kopf AJ, Wallace LM, Kimura T, Machida Y, Ide S, Davis E, IODP Expedition 365 shipboard scientists (2017) Recurring and triggered slow-slip events near the trench at the Nankai Trough subduction megathrust. Science 356:1157–1160. https://doi.org/10.1126/science.aan3120
Beeler NM, Tullis TE, Blanpied ML, Weeks JD (1996) Frictional behavior of large displacement experimental faults. J Geophys Res 101(B4):8697–8715. https://doi.org/10.1029/96JB00411
Bedford JD, Faulkner DR, Allen MJ, Hirose T (2021) The stabilizing effect of high pore-fluid pressure along subduction megathrust faults: Evidence from friction experiments on accretionary sediments from the Nankai Trough. Earth Planet Sci Lett 574:117161. https://doi.org/10.1016/j.epsl.2021.117161

Bedford JD, Faulkner DR, Lapusta N (2022) Fault rock heterogeneity can produce fault weakness and reduce fault stability. Nat Commun 13:326. https://doi.org/10.1038/s41467-022-27998-2

Behnsen J, Faulkner DR (2012) The effect of mineralogy and effective normal stress on frictional strength of sheet silicates. J Struct Geol 42:49–61. https://doi.org/10.1016/j.jsg.2012.06.015

Boulton C, Niemeijer AR, Hollis CJ, Townend J, Raven M, Kulhanek DK, Shepherd CL (2019) Temperature-dependent frictional properties of heterogeneous Hikurangi Subduction Zone input sediments, ODP Site 1124. Tectonophysics 757:123–139. https://doi.org/10.1016/j.tecto.2019.02.006

Brown KM, Kopf AJ, Underwood MB, Weinberger JL (2003) Compositional and fluid pressure controls on the state of stress on the Nankai subduction thrust: a weak plate boundary. Earth Planet Sci Lett 214(3–4):589–603. https://doi.org/10.1016/S0012-821X(03)00388-1

den Hartog SAM, Spiers CJ (2013) Influence of subduction zone conditions and gouge composition on frictional slip stability of megathrust faults. Tectonophysics 600:75–90. https://doi.org/10.1016/j.tecto.2012.11.006

Deng X, Underwood MB (2001) Abundance of smectite and the location of a plate-boundary fault, Barbados accretionary prism. Geol Soc Am Bull 113:495–507. https://doi.org/10.1130/0016-7606(2001)113%3c0495:AOSATL%3e2.0.CO;2

Dieterich JH (1979) Modeling of rock friction: 1. Experimental results and constitutive equations. J Geophys Res 84:2161–2168. https://doi.org/10.1029/JB084iB05p02161

Dieterich JH, Kilgore BD (1994) Direct observation of frictional contacts: new insights for state-dependent properties. Pure Appl Geophys 143:283–302. https://doi.org/10.1007/BF00874332

Heki K, Miyazaki S (2001) Plate convergence and long-term crustal deformation in central Japan. Geophys Res Lett 28(12):2313–2316. https://doi.org/10.1029/2000GL012537

Hirose T, Hamada Y, Tanikawa W, Kamiya N, Yamamoto Y, Tsuji T, Kinoshita M, Heuer B, Inagaki F, Morono Y, Kubo Y (2021) High fluid-pressure patches beneath the décollement: a potential source of slow earthquakes in the Nankai Trough off Cape Muroto. J Geophys Res 126:e2021JB021831. https://doi.org/10.1029/2021JB021831

Hori T, Kato N, Hirahara K, Baba T, Kaneda Y (2004) A numerical simulation of earthquake cycles along the Nankai Trough in southwest Japan: lateral variation in frictional property due to the slab geometry controls the nucleation position. Earth Planet Sci Lett 228:215–226. https://doi.org/10.1016/j.epsl.2004.09.033

Ikari MJ, Saffer DM, Marone C (2007) Effect of hydration state on the frictional properties of montmorillonite-based fault gouge. J Geophys Res 112:B06423. https://doi.org/10.1029/2006JB004748

Ikari MJ, Saffer DM (2011) Comparison of frictional strength and velocity dependence between fault zones in the Nankai accretionary complex. Geochem Geophys Geosys 12(4):Q0AD11. https://doi.org/10.1029/2010GC003442

Ikari MJ, Niemeijer AR, Marone C (2011) The role of fault zone fabric and lithification state on frictional strength, constitutive behavior, and deformation microstructure. J Geophys Res 116:B08404. https://doi.org/10.1029/2011JB008264

Ikari MJ, Hüpers A, Kopf AJ (2013a) Shear strength of sediments approaching subduction in the Nankai Trough, Japan as constraints on forearc mechanics. Geochem Geophys Geosyst 14:2716–2730. https://doi.org/10.1002/ggge.20156

Ikari MJ, Niemeijer AR, Spiers CJ, Kopf AJ, Saffer DM (2013b) Experimental evidence linking slip instability with seafloor lithology and topography at the Costa Rica convergent margin. Geology 41:891–894. https://doi.org/10.1130/G33956.1

Ikari MJ, Kameda J, Saffer DM, Kopf AJ (2015) Strength characteristics of Japan Trench borehole samples in the high-slip region of the 2011 Tohoku-Oki earthquake. Earth Planet Sci Lett 412:5–41. https://doi.org/10.1016/j.epsl.2014.12.014

Ikari MJ, Kopf AJ (2017) Seismic potential of weak, near-surface faults revealed at plate tectonic slip rates. Sci Adv 3(11):e1701269. https://doi.org/10.1126/sciadv.1701269

Ikari MJ, Kopf AJ, Hüpers A, Vogt C (2018) Lithologic control of frictional strength variations in subduction zone sediment inputs. Geosphere 14(2):604–625. https://doi.org/10.1130/GES01546.1

Ikari MJ, Hüpers A (2021) Velocity-weakening friction induced by laboratory-controlled lithification. Earth Planets Space 554:116682. https://doi.org/10.1016/j.epsl.2020.116682

Ito Y, Obara K (2006) Very low frequency earthquakes within accretionary prisms are very low stress-drop earthquakes. Geophys Res Lett 33:L09302. https://doi.org/10.1029/2006GL025883

Katayama I, Kubo T, Sakuma H, Kawai K (2015) Can clay minerals account for the behavior of non-asperity on the subducting plate interface? Prog Earth Planet Sci 2:30. https://doi.org/10.1186/s40645-015-0063-4

Kodaira S, Iidaka T, Kato A, Park JO, Iwasaki T, Kaneda Y (2004) High pore fluid pressure may cause silent slip in the Nankai Trough. Science 304(5676):1295–1298. https://doi.org/10.1126/science.1096535

Kopf A, Brown KM (2003) Friction experiments on saturated sediments and their implications for the stress state of the Nankai and Barbados subduction thrusts. Marine Geol 202:193–210. https://doi.org/10.1016/S0025-3227(03)00286-X

Kopf A (2013) Effective strength of incoming sediments and its implications for plate boundary propagation: Nankai and Costa Rica as type examples of accreting vs. erosive convergent margins. Tectonophysics 608:958–969. https://doi.org/10.1016/j.tecto.2013.07.023

Kitajima H, Hirose T, Ikari MJ, Kanagawa K, Kimura G, Kinoshita M, et al. (2020) Site C0002. In: Proc IODP, vol 358. https://doi.org/10.14379/iodp.proc.358.103.2020

Kitamura M, Hirose T, Lei X (2021) Mechanical weakness of the Nankai accretionary prism: Insights from Vp measurements of drill cuttings. Geochem Geophys Geosyst 22:e2020GC009536. https://doi.org/10.1029/2020GC009536

Kurzawski RM, Stipp M, Niemeijer AR, Spiers CJ, Behrmann JH (2016) Earthquake nucleation in weak subducted carbonates. Nat Geosci 9:717–722. https://doi.org/10.1038/ngeo2774

Loveless JP, Meade BJ (2010) Geodetic imaging of plate motions, slip rate, and partitioning of deformation in Japan. J Geophys Res 115:B02410. https://doi.org/10.1029/2008JB006248

Marone C (1998) Laboratory-derived friction laws and their application to seismic faulting. Annu Rev Earth Planet Sci 26:643–696. https://doi.org/10.1146/annurev.earth.26.1.643

Moore JC, Saffer DM (2001) Updip limit of the seismogenic zone beneath the accretionary prism of southwest Japan: an effect of diagenetic to low-grade metamorphic processes and increasing effective stress. Geology 29(2):183–186. https://doi.org/10.1130/0091-7613(2001)029%3c0183:ULOTSZ%3e2.0.CO;2

Moore DE, Lockner DA (2007) Friction of the smectite clay montmorillonite. In: Dixon T, Moore C (eds) The Seismogenic zone of subduction thrust faults. Columbia Univ. Press, New York, pp 317–345

Morrow C, Radney B, Byerlee J (1992) Frictional strength and the effective pressure law of montmorillonite and illite clays. In: Evans B, Wong T-F (eds) Fault mechanisms and transport properties of rocks. Elsevier, New York, pp 69–88

Morrow CA, Moore DE, Lockner DA (2017) Frictional strength of wet and dry montmorillonite. J Geophys Res 122(5):3392–3409. https://doi.org/10.1002/2016JB013658

Namiki Y, Tsutsumi A, Ujiie K, Kameda J (2014) Frictional properties of sediments entering the Costa Rica subduction zone offshore the Osa Peninsula: implications for fault slip in shallow subduction zones. Earth Planets Space 66:72. https://doi.org/10.1186/1880-5981-66-72

Noda H, Shimamoto T (2009) Constitutive properties of clayey fault gouge from the Hanaore fault zone, southwest Japan. J Geophys Res 114:B04409. https://doi.org/10.1029/2008JB005683

Obara K, Kato A (2020) Connecting slow earthquakes to huge earthquakes. Science 353(6296):253–257. https://doi.org/10.1126/science.aaf1512

Okuda H, Ikari MJ, Roesner A, Stanislowski K, Hüpers A, Yamaguchi A, Kopf AJ (2021) Spatial patterns in frictional behavior of sediments along the Kumano transect in the Nankai Trough. J Geophys Res 126:e2021JB022546. https://doi.org/10.1029/2021JB022546

Oohashi K, Hirose T, Takahashi M, Tanikawa W (2015) Dynamic weakening of smectite-bearing faults at intermediate velocities: Implications for subduction zone earthquakes. J Geophys Res 120(3):1572–1586. https://doi.org/10.1002/2015JB011881

Remitti F, Smith SAF, Mittempergher S, Gualtieri AF, Di Toro G (2015) Frictional properties of fault zone gouges from the J-FAST drilling project (Mw 9.0

2011 Tohoku-Oki earthquake). Geophys Res Lett 42:2691–2699. https://doi.org/10.1002/2015GL063507
Roesner A, Ikari MJ, Saffer DM, Stanislowski K, Eijsink AM, Kopf AJ (2020) Friction experiments under in-situ stress reveal unexpected velocity-weakening in Nankai accretionary prism samples. Earth Planet Sci Lett. https://doi.org/10.1016/j.epsl.2020.116180
Ruina AL (1983) Slip instability and state variable friction laws. J Geophys Res 88:10359–10370. https://doi.org/10.1029/JB088iB12p10359
Rubin AM (2008) Episodic slow slip events and rate-and-state friction. J Geophys Res 113:B11414. https://doi.org/10.1029/2008JB005642
Saffer DM, Marone C (2003) Comparison of smectite- and illite-rich gouge frictional properties: application to the updip limit of the seismogenic zone along subduction megathrusts. Earth Planet Sci Let 215(1–2):219–235. https://doi.org/10.1016/S0012-821X(03)00424-2
Schnaid F, Prietto PDM, Consoli NC (2001) Characterization of cemented sand in triaxial compression. J Geotech Geoenviro Eng 127(10):857–868. https://doi.org/10.1061/(ASCE)1090-0241
Scholz CH (2002) The mechanics of earthquake and faulting, 2nd edn. Cambridge University Press
Skarbek RM, Savage HM (2019) RSFit3000: A MATLAB GUI-based program for determining rate and state frictional parameters from experimental data. Geosphere 15(5):1665–1676. https://doi.org/10.1130/GES02122.1
Shibazaki B, Shimamoto T (2007) Modelling of short-interval silent slip events in deeper subduction interfaces considering the frictional properties at the unstable-stable transition regime. Geophys J Int 171:191–205. https://doi.org/10.1111/j.1365-246X.2007.03434.x
Shiraishi K, Yamada Y, Nakano M, Kinoshita M, Kimura G (2020) Three-dimensional topographic relief of the oceanic crust may control the occurrence of shallow very-low-frequency earthquakes in the Nankai Trough of Kumano. Earth Planets Space 72:72. https://doi.org/10.1186/s40623-020-01204-3
Stipp M, Rolfs M, Kitamura Y, Behrmann JH, Schumann K, Schulte-Kortnack D, Feeser V (2013) Strong sediments at the deformation front, and weak sediments at the rear of the Nankai accretionary prism, revealed by triaxial deformation experiments. Geochem Geophys Geosyst 14(11):4791–4810. https://doi.org/10.1002/ggge.20290
Sugioka H, Okamoto T, Nakamura T, Ishihara Y, Ito A, Obana K et al (2012) Tsunamigenic potential of the shallow subduction plate boundary inferred from slow seismic slip. Nature Geosci 5(6):414–418. https://doi.org/10.1038/ngeo1466
Takahashi M, Azuma S, Ito H, Kanagawa K, Inoue A (2014) Frictional properties of the shallow Nankai Trough accretionary sediments dependent on the content of clay minerals. Earth Planets Space 66:75. https://doi.org/10.1186/1880-5981-66-75
Tembe S, Lockner DA, Wong TF (2010) Effect of clay content and mineralogy on frictional sliding behavior of simulated gouges: binary and ternary mixtures of quartz, illite, and montmorillonite. J Geophys Res 115:B03416. https://doi.org/10.1029/2009JB006383
Tetsuka H, Katayama I, Sakuma H, Tamura K (2018) Effects of humidity and interlayer cations on the frictional strength of montmorillonite. Earth Planets Space 70:56. https://doi.org/10.1186/s40623-018-0829-1
Tobin H, Hirose T, Saffer DM, Toczko S, Maeda L, Kubo Y, the Expedition 348 Scientists (2015) Site C0002. In: Proc IODP, vol 348. https://doi.org/10.2204/iodp.proc.348.103.2015
Tobin H, Hirose T, Ikari M, Kanagawa K, Kimura G, Kinoshita M, Kitajima H, Saffer D, Yamaguchi A, Eguchi N, Maeda L, Toczko S, the Expedition 358 Scientists (2020) Expedition358 summary. In: Proc IODP, vol 358. https://doi.org/10.14379/iodp.proc.358.101.2020
Tsutsumi A, Fabbri O, Karpoff AM, Ujiie K, Tsujimoto A (2011) Friction velocity dependence of clay-rich fault material along a megasplay fault in the Nankai subduction zone at intermediate to high velocities. Geophys Res Lett 38:L19301. https://doi.org/10.1029/2011GL049314
Underwood MB (2017a) Data report: clay mineral assemblages in cuttings from Hole C0002N, IODP Expedition 348, Nankai Trough accretionary prism. In: Proc IODP, vol 348. https://doi.org/10.2204/iodp.proc.348.203.2017a
Underwood MB (2017b) Data report: clay mineral assemblages and illite/smectite diagenesis in cuttings from Hole C0002P, IODP Expedition 348, Nankai Trough accretionary prism. In: Proc IODP, vol 348. https://doi.org/10.2204/iodp.proc.348.204.2017b
Yokota Y, Ishikawa T (2020) Shallow slow slip events along the Nankai Trough detected by GNSS-A. Sci Adv 6(3):eaay5786. https://doi.org/10.1126/sciadv.aay5786

Publisher's Note